MULTI-MODALITY CT-PET-NIR FLUORESCENCE TOMOGRAPHY

A. Joshi,[†1] *J.C. Rasmussen,*[†] *S. Kwon,*[†] *T.A. Wareing,*[††] *J. McGhee,*[††] *and E.M. Sevick-Muraca*[†2]

[†]Department of Radiology, Baylor College of Medicine, Houston, Texas
[††]Transpire Inc., Gig Harbor, Washington

ABSTRACT

We report the development of a multi-modality NIR fluorescence tomography system. Existing small animal imaging techniques of micro CT and micro PET are utilized to acquire the animal geometry from which a finite element description of animal body is created. Non-contact frequency domain fluorescence boundary measurements are acquired by positioning a scanning NIR laser source and a gain modulated intensified CCD camera in a rotational mode about the animal bed used in the CT/PET scanner. Optical imager is aligned with the PET gantry to enable seamless imaging. Fluorescence image reconstruction is performed with the help of a novel radiative transport theory based algorithm. We demonstrate 3D image reconstruction of a multi-modality CT/PET/Fluroescence target implanted within the torso of a nude mouse.

Index Terms— Frequency domain optical tomography, multi-modality small animal imaging

1. INTRODUCTION

Small animal imaging plays an integral role in elucidating the biomolecular aspects of disease and health, as well as in confirming the *in vivo* molecular action of therapeutic drug candidates. While nuclear medicine with SPECT and PET imaging continues to offer the "gold standards" of molecular imaging owing to the high sensitivity and tissue depth penetration of radiolabeled molecular probes, the convenience associated with fluorescence labels suggests a prominent role of optical imaging in drug discovery. In addition, the functional imaging ability of fluorescence probes complements the high resolution structural imaging provided by X ray CT or microMRI. While, a number of small animal optical imaging systems have been reported, [1, 2, 3] a seamless integration of existing structural and nuclear imaging techniques with fluorescence optical imaging has not been yet demonstrated. In this contribution, we report the development of a frequency domain fluorescence imaging system which seamlessly integrates with existing microCT/SPECT/PET systems. Transmission mode fluorescence measurements are acquired in a non-contact manner. Non-contact measurements as well as the physical constraints of imaging small animals like nude mice do not allow the direct application of prevalent photon diffusion theory based image reconstruction algorithms. We employ a novel numerical solver for coupled frequency domain Boltzman radiative transport equations(RTE) for simulating the forward and adjoint photon flux needed by iterative reconstruction algorithms. Previously reported RTE based fluorescence optical tomography algorithm utilize discrete ordinates step/diamond differencing solution schemes. [4] In this contribution, we demonstrate for the first time model based frequency domain fluorescence optical tomography with a proven RTE solver which couples the discrete ordinates or S_N methods to a discontinuous Galerkin finite element method (DGFEM) based spatial differencing scheme. Our approach allows the use of unstructured tetrahedral meshes generated from microCT or PET transmission scans to describe arbitrary small animal geometries. The accuracy of RTE solution with DGFEM differencing schemes is mesh independent, hence allowing the use of coarser meshes and the resulting savings in computation time. We describe the hybrid imaging system in section-2, the RTE based tomography algorithm in section-3, and an image reconstruction example in section-4.

2. MATERIALS AND METHODS

Imaging System The schematic of the hybrid imaging system is depicted in Figure 1. The animal is positioned on a custom designed bed which is compatible with Seimens microCT/SPECT as well as the Inveon microPET system. The animal bed motion through the gantry is controlled from the CT/PET scanner user interface. The animal weight is supported by a thin wire mesh to allow NIR illumination from the bottom. After acquiring the CT and/or PET scan, the bed is advanced outside the bore of the PET scanner and into the field of view of the optical imager. An NIR laser diode positioned on a mobile platform is collimated to project a point on the animal surface. The laser diode is modulated at $100MHz$. Images at excitation and emission wavelengths are acquired by the intensified CCD camera system positioned on the transmission side, by using suitable optical filters. The image intensifier is also modulated at $100MHz$ by a sec-

[1]Contact author: amitj@bcm.edu, supported by NIH grant R42 CA115028

[2]Supported by NIH grant R01 EB003132

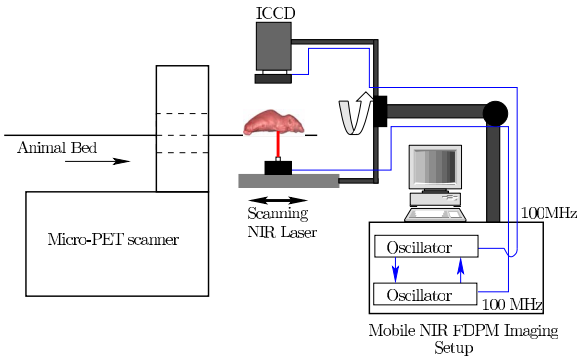

Fig. 1. Multimodality Imaging Setup: The optical imaging system comprising of a scanning NIR laser source and image intensified CCD camera system is positioned on a mobile cart and aligned with the animal bed and motion apparatus of the microPET scanner

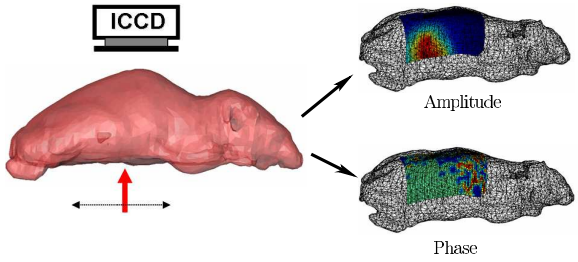

Fig. 2. Registration of Fluorescence amplitude and phase measurements onto the tetrahedral mesh generated from microCT scan

ond oscillator and the amplitude and phase images of excitation/fluorescence are obtained with the Homodyne technique. [5] The laser source and camera can be rotated to acquire multiple projections of the animal.

Multi-modality data registration In order to solve the RTE model based fluorescence tomography, the animal geometry needs to be known and co-registered with the planar images acquired with the CCD camera. The CT scan provides animal anatomy in great detail, while the PET transmission scan can also provide a low resolution image which is sufficient for extracting the animal perimeter. The structural images are segmented and meshed in the visualization environment AMIRA. Fiducial markers placed on the animal bed are used to create a common coordinate system for the animal body mesh and the NIR source position. The CCD camera measurements are treated as projections of true measurements on the animal surface and registered with the triangular boundary faces of the animal body mesh for each projection.(Figure 2)

3. RTE BASED FLUORESCENCE TOMOGRAPHY

For brevity, we write the coupled frequency domain excitation and emission RTE as a block linear system:

$$\begin{bmatrix} H_x & 0 \\ -B_{xm} & H_m \end{bmatrix} \begin{bmatrix} \widetilde{\Phi}_x \\ \widetilde{\Phi}_m \end{bmatrix} = \begin{bmatrix} S_{ex} \\ 0 \end{bmatrix} \quad (1)$$

$$H_{x,m} = \mathbf{\Omega} \cdot \nabla \widetilde{\Phi}_{x,m} + \left[\Sigma_T^{x,m}(\mathbf{r}) + \frac{i\omega}{c_{x,m}} \right] - Q_{scat}^{x,m} \quad (2)$$

$$B_{xm}\widetilde{\Phi}_x = \frac{1}{4\pi} \int_{4\pi} \frac{\eta(\mathbf{r})}{1 + i\omega\tau(\mathbf{r})} \widetilde{\Phi}_x(\mathbf{r}, \mathbf{\Omega}, \omega) d\mathbf{\Omega} \quad (3)$$

$$Q_{scat}^{x,m} = \mu_s^{x,m}(\mathbf{r}) \int_{4\pi} p(\mathbf{\Omega} \cdot \mathbf{\Omega}') \widetilde{\Phi}_{x,m}(\mathbf{r}, \mathbf{\Omega}', \omega) d\mathbf{\Omega}' \quad (4)$$

$$\Sigma_T^{x,m}(\mathbf{r}) = \mu_s^{x,m}(\mathbf{r}) + \mu_{ai}^{x,m}(\mathbf{r}) + \mu_{af}^{x,m}(\mathbf{r}) \quad (5)$$

$$\eta(\mathbf{r}) = \nu(\mathbf{r})\mu_{af}^{x}(\mathbf{r})$$

Here H denotes the transport operator, subscripts x, m represent excitation and emission wavelengths respectively. B_{xm} is the term coupling the excitation RTE with the emission RTE and it depends upon the quantum yield $(\nu(\mathbf{r})\mu_{af}^{x}(\mathbf{r}))$ and the lifetime $\tau(\mathbf{r})$ of the fluorescence probe employed. The NIR light transport in tissue is governed by the absorption μ_a and scattering μ_s cross-sections. Subscript i denotes the properties of endogenous chromophores, while subscript f denotes the properties of exogenous fluorophores. $Q_{scat}^{x,m}$ is the scattering source which depends upon the probability $p(\mathbf{\Omega} \cdot \mathbf{\Omega}')$ of scattering of a photon from the direction $\mathbf{\Omega}$ to $\mathbf{\Omega}'$. S_{ex} is the externally applied excitation source. The coupled RTE system (1) can be solved to obtain the angular fluence $\widetilde{\Phi}$ at excitation and emission wavelengths.

Forward Solver The transport equation solver for optical fluorescence modelling was developed on top of a pre-existing general purpose radiation transport analysis system Attila™ (Transpire Inc. Gig Harbor, WA, USA). Attila™ was initially developed at the Los Alamos National Laboratory [6], Los Alamos, NM, USA. In Attila™ numerical solution of transport equation involves two steps: (i) angular discretization by discrete ordinates method, (ii) spatial discretization by discontinuous finite element based differencing and the solution of the resulting linear systems with source iteration method coupled with diffusion synthetic acceleration(DSA). A high order angular quadrature set is needed to avoid ray effects in transport equation solutions for weakly scattering media. Most biological tissues are strongly scattering and a low order angular approximation provides sufficient accuracy. However, for imaging applications in which the animal is surrounded by non-scattering media and a non-contact illumination is used, a higher order quadrature is necessary to resolve the transport of excitation photons to the animal boundary. These computations can be carried out efficiently by breaking the transport calculation in two stages: (i) computing an analytical ray trace of unscattered photons

through out the imaged domain, followed by (ii) a low angular quadrature based numerical transport solution with the uncollided photons acting as external sources of photons. For the imaging setup depicted in Figure (1), the NIR source is analytically described for computing the unscattered photon flux through the animal body. The RTE solution procedure and its experimental validation is described in detail in references [7] and [8]

Inverse Solver The general fluorescence tomography problem involves the determination of discretized fluorescence absorption coefficient $\mu_{\mathbf{af}}^{\mathbf{x}} = \{\mu_{af_i}^{x}\}, i = 1, 2...N$ from a set of discrete boundary measurements of scalar emission fluence $\mathbf{z} = \{z_j\}, j = 1, 2...M$, where z_j is defined as: $z_j = \int_{\theta_j} \widetilde{\Phi}_m^j$. θ_j is the angular aperture of the j^{th} photon collector. The measurements $\mathbf{z}$ depend nonlinearly on the unknown fluorescence absorption $\mu_{\mathbf{af}}^{\mathbf{x}}$. The tomography problem can be linearized if a first order Taylor series expansion about a initial fluorescence map $\mu_{\mathbf{af_0}}^{\mathbf{x}}$ is used to describe the boundary fluorescence measurements:

$$\mathbf{z} - \mathbf{z}_0 = \mathbf{J} \cdot \left(\mu_{\mathbf{af}}^{\mathbf{x}} - \mu_{\mathbf{af_0}}^{\mathbf{x}}\right) \quad \mathbf{J} = \left[\frac{\partial \mathbf{z}}{\partial \mu_{\mathbf{af}}^{\mathbf{x}}}\right]_{\mu_{\mathbf{af}}^{\mathbf{x}} = \mu_{\mathbf{af_0}}^{\mathbf{x}}} \tag{6}$$

Where $\mathbf{J}$ is the jacobian sensitivity matrix with dimensions of MxN, where M is the number of measurements and N is the number of unknowns. Calculation of the Jacobian matrix dominates the computational cost of typical optical tomography algorithms. $\mathbf{J}$ can be efficiently computed by employing the adjoint transport equation. We define the adjoint system for j^{th} detector with response D_j as:

$$\begin{bmatrix} H_x^* & -B_{xm}^* \\ 0 & H_m^* \end{bmatrix} \begin{bmatrix} \widetilde{\Psi}_x^j \\ \widetilde{\Psi}_m^j \end{bmatrix} = \begin{bmatrix} 0 \\ D_j \end{bmatrix} \tag{7}$$

Here, $H_{x,m}^*$ are the adjoint transport operators. For vacuum boundary conditions, H^* is defined as:

$$H_{x,m}^* = -\mathbf{\Omega} \cdot \nabla \widetilde{\Phi}_{x,m} + \left[\Sigma_T^{x,m}(\mathbf{r}) - \frac{i\omega}{c_{x,m}}\right] - Q_{scat}^{x,m} \tag{8}$$

The adjoint operator B_{xm}^* is obtained by taking the complex transpose of B_{xm}

$$B_{xm}^* \widetilde{\Psi}_m = \frac{1}{4\pi} \int_{4\pi} \frac{\nu(\mathbf{r})\mu_{af}^x(\mathbf{r})}{1 - i\omega\tau(\mathbf{r})} \widetilde{\Psi}_x d\mathbf{\Omega} \tag{9}$$

It can be observed that the adjoint transport operator for photon propagation in frequency domain is reversed in direction and time(phase) with respect to the forward operators. The jk^{th} element of the Jacobian matrix can then be expressed in terms of the adjoint solutions $\widetilde{\Psi}_{x,m}$ by exploiting the definition of the adjoint operator:

$$J_{jk} = < D_j, \frac{\partial \widetilde{\Phi}_m}{\partial \mu_{af_k}^x} > = < \widetilde{\Psi}_x^j, \frac{\partial H_x}{\partial \mu_{af_k}^x} \widetilde{\Phi}_x > \tag{10}$$

$$+ < \widetilde{\Psi}_m^j, \frac{\partial B_{xm}}{\partial \mu_{af_k}^x} \widetilde{\Phi}_x > \tag{11}$$

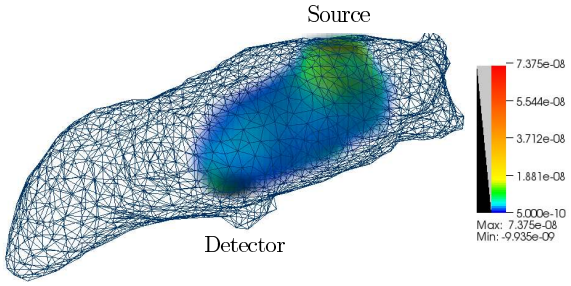

Fig. 3. Illustration of a row of jacobian matrix J. The color scale indicates the sensitivity of a given source-detector pair measurement to the unknown fluorescence absorption map defined on the finite element mesh of the animal body.

The first term on the R.H.S of equation (10) can be dropped upon invoking the Born approximation, wherein the excitation field is assumed not to be perturbed by the presence of fluorescent target. The adjoint solution $\widetilde{\Psi}_m^j$ does not depend on the particular image voxel index k, hence in a linearized tomography algorithm, the adjoint solutions $\widetilde{\Psi}_m^j$ can be precomputed and stored for all M collector locations. The Jacobian matrix can then be assembled on demand provided the forward solutions $\widetilde{\Phi}_x$ corresponding to all excitation sources are available. The computation of the terms $\partial B_{xm}/\partial \mu_{af_k}^x$ depends upon the discretization scheme employed, but it is straightforward as the operator B_{xm} depends linearly on μ_{af}^x. In fact, $\mathbf{J}$ doesn't even need to be explicitly constructed. Iterative solution methods such as algebraic reconstruction technique or conjugate gradient least squares, only require matrix-vector products involving $\mathbf{J}$, and they can be implemented directly with equation (10) once the respective forward and adjoint RTE solutions are available. For the system described in Figure 1, the pixels on the CCD images projected to the animal surface as shown in Figure 2 are treated as detectors. Figure 3 depicts the volume rendering of a typical row of the Jacobian matrix, with the point source illuminating the top surface.

4. MULTI-MODALITY IMAGE RECONSTRUCTION

To validate the multi-modality small animal imaging hardware and software, a 3-4mm glass bulb was implanted in the carcass of a nude mouse. The bulb was filled with a CT contrast agent $Fenestra^{TM}$, PET agent FDG, and 12 nanomoles of fluorescent dye Indocyanine Green. CT, PET and optical scans were acquired in that order. For the optical scan, only two projections at 180 degrees were acquired to limit the data acquisition time. The jacobian matrix was assembles with 400 detector points and 10 source positions for each projection. This requires 800 adjoint RTE computations and 20 forward RTE computations, however as these calculations are independent of each other, they were implemented in parallel

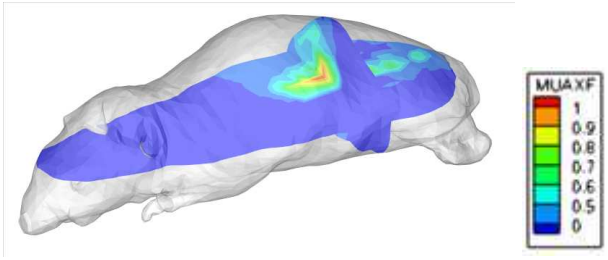

Fig. 4. Fluorescence reconstruction: Orthogonal slices drawn through the reconstructed fluorescence absorption map are depicted. The fluorescent bulb is identified.

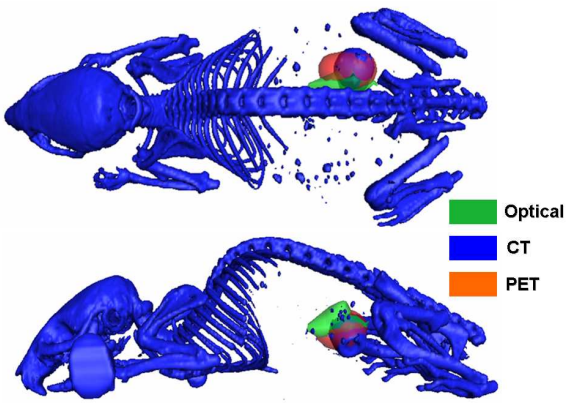

Fig. 5. Isosurfaces drawn through the CT, PET, and fluorescence reconstructed images.

on a Linus Beowulf cluster with 32 AMD opteron processors (2.2 GHz) and 4 GB of system memory per processor. The total time for the Jacobian computation was under 45 minutes. The forward and adjoint computations were conducted under the assumption that the entire mouse was homogenous and the endogenous absorption and scattering cross-sections were taken to be equal to murine muscle properties reported in literature. [9] The linear system (6) was inverted with LSQR method in MATLAB.

Figure 4 depicts the slices drawn through the reconstructed fluorescence absorption map through the mouse body. The image resolution was limited by the coarse mesh employed to limit the computation time. Figure 5 depicts the co-registered CT/PET and fluorescence tomographic images. Isosurfaces are drawn through the CT image to highlight the skeletal structure and the Fenestra filled glass bulb. The isosurfaces through the PET and fluorescence images are drawn at 80% of the maximum contour level. The fluorescence isosurface is shifted with respect to the CT/PET reconstruction. This may be because of multiple reasons, including inexact boundary conditions for RTE, optical imager motion during the fluorescence data acquisition, and the use of averaged optical properties.

5. CONCLUSIONS AND FUTURE WORK

This contribution marks our first step towards hybrid structural-molecular small animal tomography systems, which utilize animal structure information from established modalities like Xray CT, and seek to determine the distribution of molecularly targeting fluorescence probes without exact *a priori* information of interior endogenous optical properties. Current work is focused on the implementation of exact boundary conditions for coupled RTE's and reducing the data acquisition time to allow the acquisition of fluorescence measurements from more than two projections.

6. REFERENCES

[1] A.T. Kumar, S.B. Raymond, G. Boverman, D.A. Boas, and B.J. Bacskai. Time resolved fluorescence tomography of turbid media based on lifetime contrast. *Optics Express*, 14(25):12255–12270, 2006.

[2] S. Patwardhan, S. Bloch, S. Achilefu, and J. Culver. Time-dependent whole-body fluorescence tomography of probe bio-distributions in mice. *Optics Express*, 13(7):2564–2577, 2005.

[3] N. Deliolanis, T. Lasser, D. Hyde, A. Soubret, J. Ripoll, and V. Ntziachristos. Free-space fluorescence molecular tomography utilizing 360 geometry projections. *Optics Letters*, 32(4):382–384, 2007.

[4] A. Klose and A. H. Hielscher, "Fluorescence tomography with simulated data based on the equation of radiative transfer," *Opt. Lett.*, vol. 28, no. 12, pp. 1019–1021, 2003.

[5] J. S. Reynolds, T. L. Troy, and E. M. Sevick-Muraca, "Multi-pixel techniques for frequency-domain photon migration imaging," *Biotechnolgy Progress*, vol. 13, pp. 669–680, 1997.

[6] TA Wareing, JM McGhee, and JE Morel. Attila: A three dimensional unstructured tetrahedral mesh discrete ordinates transport code. *Transactions of the American Nuclear Society*, 75:146–147, 1996.

[7] J.C. Rasmussen, A. Joshi, T. Pan, T. Wareing, J. McGhee, and E.M. Sevick-Muraca. Radiative transport in fluorescence-enhanced frequency domain photon migration. *Medical Physics*, 33:4685, 2006.

[8] A. Joshi, J.C. Rasmussen, E.M. Sevick-Muraca., T. Wareing, and J. McGhee Radiative Transport Based Frequency Domain Fluorescence Tomography. *Physics in Medicine and Biology*, submitted 2007.

[9] WF Cheong, SA Prahl, and AJ Welch. A review of the optical properties of biological tissues. *Quantum Electronics, IEEE Journal of*, 26(12):2166–2185, 1990.